NUMERICAL INVESTIGATIONS OF BOUNDARY LAYER FLOWS AND HEAT TRANSFER OF CROSS FLUID

By

MAZHAR SHEHZAD

(Fall 2016-MS CS&E-9 00000173018)

Supervisor: Dr. Ammar Mushtaq

Research Center for Modeling and Simulation (RCMS)

National University of Sciences and Technology (NUST)

Sector H-12, Islamabad, Pakistan

August, 2020

NUMERICAL INVESTIGATIONS OF BOUNDARY LAYER FLOWS AND HEAT TRANSFER OF CROSS FLUID

A thesis submitted in partial fulfillment of the requirements
for the degree of Master of Science in Computational Science and Engineering

By

Mazhar Shehzad

Fall 2016-MS CS&E 00000173018

Supervisor: Dr. Ammar Mushtaq

Research Center for Modeling and Simulation (RCMS)
National University of Sciences and Technology (NUST)
Sector H-12, Islamabad, Pakistan

August, 2020

Dedication

I am dedicating this thesis to first and foremost my beloved father who has meant and continues to mean so much to me. Although he is no longer of this world, his memories continue to regulate my life. Whose love for me knew no bounds and, who taught me the value of hard work.

I also dedicate wholeheartedly this work to my mother, who has a source of inspiration and gave me strength when I taught of giving up, who continuously provides her moral, spiritual, and financial support.

I also dedicate this work to Nazar Malik (DD finance, NUST) who shared his words of advice and encouragement to finish this study.

And finally to my brother, sister, and mentor whose encouragement has made sure that I give it all it takes to finish that which I have started.

Acknowledgments

Throughout the writing of the thesis, I have received a great deal of support and assistance. I would first like to thank my thesis advisor Dr. Ammar Mushtaq (RCMS, NUST). The door to Dr. Ammar office was always open whenever I ran into a trouble spot or had a question about my research or writing. The expertise was invaluable in the formulating of the research topic and methodology in particular. He consistently gave me confidence and steered me in the right direction whenever he thought I needed it.

I would also like to thank the learned faculty who were involved in this research project. Dr. Junaid Ahmad Khan (RCMS, NUST), Dr. Adnan Maqsood (RCMS, NUST), Dr. Salma Sherbaz (RCMS, NUST) without their passionate participation and input, and provided me with the tools that I needed to choose the right direction.

In addition, I would like to thank Principal RCMS and my family for their wise counsel. You were always there for me. Finally, there are my friends, who were of great support in deliberating over our problems and findings, as well as providing a happy distraction to rest my mind outside of my research.

Table of Contents

Abstract

During the past century, rheology has emerged as a new science which deals with the deformation of the matter. Metal spinning, wire drawing, polymer extrusion, blood circulation, food industry, and pressure-sensitive adhesion, etc are a few of the potential application areas. Now in most of these applications materials are Non-Newtonian and involve rotation, extrusion, and heat exchange. Therefore, understanding the rheology is critically important in order to improve the quality of product development, methodology, and resource utilization.

The goal of this research is to present the boundary layer equations for fluid flow and heat transfer of cross fluid over a moving flat plate. The job is further expanded to cover a stretched surface with the rotating stream of cross fluid. The systems of governing partial differential equations are converted into highly non-linear ordinary differential equations by introducing appropriate similarity transformations. By using the bvp4c process, the governing ODEs are solved numerically, and the influence of the related parameters of practical importance such as skin friction coefficient and Nusselt number are calculated. The momentum boundary layer demonstrates the elevation impact of the growing local Weissenberg number. The contrary phenomenon for the thermal boundary layer was found. The temperature function has an exceptional S-shaped profile indicating the existence of an adiabatic case for the large enough wall to ambient temperature ratio. Velocity fields and the structures of the momentum boundary layer demonstrated the same enhancement tendency for the rising Weissenberg number.

List of Figures

List of Tables

Chapter 1
Introduction

1.1 Motivation

An American chemistry professor first coined the term “Rheology” which he inspired from the Greek word “$\pi\alpha\nu\tau\alpha\rho\varepsilon\iota$” meaning “everything flows”. During the past century, rheology has emerged as a new science which deals with the deformation of the matter. The rheological studies are focused on dealing with applied stress and strain. As all materials have rheological properties thus rheology is relevant in many fields. Examples include metal spinning, wire drawing, concrete technology, plastic processing, polymer extrusion, paint flows, blood circulation, cosmetics, food industry, and pressure-sensitive adhesion, etc. Now understanding rheology is critically important in order to improve the quality of product development, methodology, and resource utilization. Particularly to the food industry where most materials are Non-Newtonian, Rotating flows in mixtures, extruders, and heat exchangers are widely common [1].

Owing to the above-mentioned application areas rotating, stretching flow, and heat transfer of Non-Newtonian have gained the special interest of the scientific community for the past few decades. Thus the current thesis is directed towards flow and heat transfer of Non-Newtonian fluid over flat and stretching surfaces.

1.2 Non-Newtonian Fluid

The fluids that flow Newton’s law of viscosity (Shear stress is linearly and directly proportional to deformation rate) are known as Newtonian fluid and any fluid that does not follow Newton’s Law of viscosity is a Non-Newtonian fluid. Mathematically:

$$\tau = \mu^{*}\dot{\gamma} \qquad 1.1$$

Here τ is the shear stress, μ^{*} is the effective dynamic viscosity and $\dot{\gamma}$ is the deformation rate. μ^{*} is constant for Newtonian and variable for Non-Newtonian

fluids. Fig 1.1 discusses different types of Rheological fluid models based on the behavior of their viscosity.

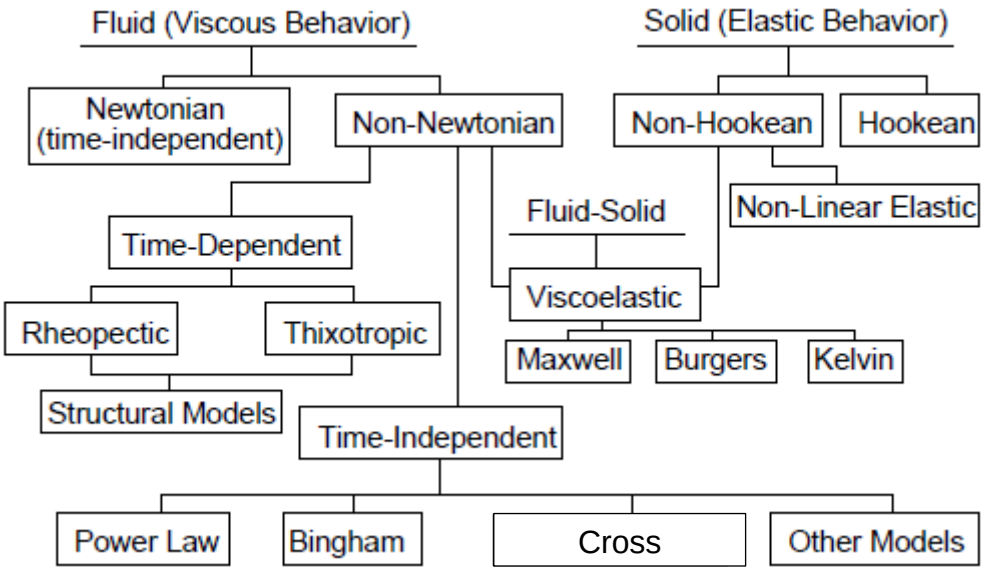

Fig 1.1 Classifications of Rheological Models[1]

1.3 Literature Review

Blasius [2], pioneered in studying the motion of flow on a stationary flat plate. Then later, Leslie Howarth proposed the theory of turbulence in aerodynamics as well as in fluid dynamics [3]. The influence of the boundary layer over a moving plate was then scrutinized by Sakiadis [4-5]. By extending the work of Sakiadis, Crane [6] was able to work for the problem of stretching flat plate and found the exact solution of boundary layer equations. But all these studies were carried out for Newtonian fluids. We need non-Newtonian fluids Because of its broad spectrum of industries applications. Various studies have been carried out on momentum and heat transfer and of non-Newtonian fluids [7-8]. Today many studies are being carried out for many other physical investigations of micropolar fluids, power law, Maxwell fluids, second-grade fluids, etc. So the complex fluids particles like suspensions, turbulent shear flows, can be described using the theory of micropolar fluid flows. [9-14] worked on micropolar and power-law fluids. The power-law model refers to non-Newtonian fluids which are time-independent. The power-law model is sufficient for many non-Newtonian fluids to explore the shear stress and shear rate measurements.

In spite, the power-law model has a strong engineering influence, but it cannot explore the normal stress differences. In this regard, we will consider a special type of differential equations of fluids for which the analytical solutions are available. These differential fluids are the class of second-grade fluids [15-17]. This model refers to determining the normal stress results. A significant amount of research on the physical analysis of the laminar boundary layer flows across solid surfaces has been published [18-25].

During the fast few decades, the study of flow in a rotating frame has increased substantially. This is because of the promising application in geophysical and cosmically fluid dynamics. Rotating flows are also crucial in solar physics Involved in sunspots growth, rotating magnetic stars, and solar cycle structures. Nanofluid flow study in rotating stretch sheets has enormous applications in industrial technology such as aerospace, rotary equipment, heat generation, rotor-stator systems, medical equipment, electronic and computer storage equipment, crystal phenomena development, air cleaning equipment, food processing technology, turbomachinery, and many more. The solution of many rotating flow problems is analyzed by understanding the behavior of boundary layers. Interesting flow analysis in a rotating system performed by authors Loper [26], Debnath [27], Gupta [28], Murthy, and Ram [29]. Keeping in view all this work is not enough progress of rotating flow for non-Newtonian flow. In this perspective, Taylor [30] interpreted a significant indication of the different viscous fluids in the rotating system. Greenspan [31] Von Karman[32] studied the hydrodynamic flow through an infinite rotating disc. In this work, Von Karman applied his prominent similarity transformations. Which descend PDEs into ODEs. Choi and Eastman [33] were probably the first to use nanoparticles and base fluid mixture and they called it "Nanofluid". Turkyilmazoglu [34-35] examined Nanofluid flow behavior with a rotating disk with heat and mass transfer impacts. Sheikholeslami et al [36-37] conducted comprehensive research on the rotational behavior of nanofluid flow using distinct developments. Hayat et al.[38] explored the rotating three-dimensional (3D) flow of carbon nanotubes with a porous medium of Darcy – Frochheimer. The pioneering author Crane [6] introduced the fluid flow through the stretch sheet. Many researchers such as Vajraelu and Roper [39] who worked on the stream of second-grade liquids and stretching sheets extended Crane's job. Rosca and Pop [40] and Sajid et al.[41] observed the vicious unstable movement as a result of a curved shrinking / stretching medium. Wang [42] implemented the

small parameter λ to study the 3-D rotating viscous flow over a stretched surface. λ indicates the ratio of the rotation-stretching rate. It is reported that the velocity distribution decays with increment in the value of λ. Study of non-Newtonian second grade rotating fluid performed by Hayat and Hutter [43] and Hayat at el. [44]. They observed a direct relationship between the fluid velocity and material parameters of the second-grade flow.

When suction or blowing is applied at the moving surface. Since the polymer is a flexible material, so the structure of the filament surface may expand during the ejection and thus the surface velocity can change from being uniform. The thermal radiation over a continually stretching surface has taken on excellent significance Due to its use in a wide range of manufacturing and scientific uses, such as the manufacture of plastics, metallurgy, crystal processing, and many others. Plastic sheet drawing. The performance of the final product relies on cooling and stretching rates. The boundary layer flows over a continuously moving surface First mentioned by Sakiadis [4]. For linear stretching sheets, Sakiadi's work was further extended by Crane. Rees and Bassom [45] predicted the flow of a micro-polar fluid over a flat plate on the Blasius boundary layer while Soundalgekar and Takhar proposed a similarity evaluation of flow and heat transfer over a continuously flowing semi-infinite plane of micro-polar fluid [46]. Turkyilmazoglu [47] has investigated the flow through a rotating disk of five specific water-based nanofluid types. Sugu-namma et Al.[48] investigated the transfer of heat from nanofluid to rotating frames influenced by the magnetic field and thermal radiation. Pramanik [49] examined the heat transfer study of the Casson fluid on a suction / blowing exponentially stretching surface and found that the friction factor for suction is greater than that for blowing.

1.4 Research Gap

The above section shows that although a huge amount of research has been carried out on the boundary layer flows for Newtonian and non-Newtonian fluids. However, to investigate the shear-thinning/thickening region most popular non-Newtonian Model used is the Power Law model. Despite its ability to present a vast class of non-Newtonian fluids, it has its limitations in presenting fluids with very high and very low shear rate. In 1965 Cross [50] introduce a model that caters to a wider sub-section

of generalized Newtonian fluids which can detect both the flow rate in the power-law region as well as the very high and very low shear rate range.

Now, with the available computing resources and advancement in numerical techniques to tackle highly nonlinear equations such as arising in modeling of Cross fluid, researchers have started working on problems with many folds complexity. Khan et al [51] reported in 2016 on boundary layer flows and the heat transfer of the cross fluid over the stretch surface. Hayat et al [52] published in 2017 worked on the numerical simulation of heat distribution to a stretched surface of stagnation point MHD of cross-fluid. In 2017 Khan et al [53] reported on cross-axisymmetric flow and heat transfer across a radially stretched surface. In 2019, Sultan et al [54] explored theoretical elements of thermophoresis and Brownian motion with the activation energy for the 3-D flow of the cross fluid. For the validations purpose the results of the power-law index against temperature profile were compared with Kumari nath[55]. Therefore, still, a lot of potential fluid scenarios can be modeled and solved for an in-depth understanding of flow and heat transfer of the Cross fluid model.

1.5 Objectives

The objectives of this research are as follows:

- To present the boundary layer equations for fluid flow and heat transfer of Cross fluid over a moving flat plate
- To extend the 2D equations into 3D equations covering extrusion and rotational effects of Cross fluid.
- To present the numerical solutions of the above-mentioned scenarios
- To discuss the effects of important parameters arising during modeling and solution of Cross fluid model; especially, practically important parameters such as skin friction, Nusselt number, and Weissenberg number.

1.6 Numerical Method

The governing differential system for fluid flow and heat transfer phenomenon is generally a non-linear Boundary-Valued Problem (BV P). The boundary value problems can be solved using the finite difference method or the iterative procedure known as the Shooting method. The later is preferred in the boundary layer flow problems because it uses a fifth-order accurate Runge-Kutta scheme whereas the

finite difference method is only second-order accurate. Other advantages of the shooting method include its simple implementation as well as its faster convergence rate when compared to other numerical integration techniques. The basic idea of the shooting method is as follows:

Consider the Blasius problem [2]

$$f''' + ff'' = 0;\ f(0) = 0;\ f'(0) = 0;\ f'(\infty) = 1 \tag{1.2}$$

In order to solve the above-mentioned higher-order differential problems numerically. First, they are converted into a system of 1st order equations using new variables. Therefore, let $y_1 = f; y_2 = f'$ and $y_3 = f''$. The equivalent first-order equations for Blasius problem are as follows:

$$y_1' = y_2; y_2' = y_3 \text{ and } y_3' = -y_1 y_3 \tag{1.3}$$

with boundary conditions

$$y_1(0) = 0;\ y_2(0) = 0;\ y_2(\infty) = 1 \tag{1.4}$$

The solution of Eq. (1.15) is obtained using the fifth-order Runge-Kutta integration technique with the following initial conditions

$$y_1(0) = 0;\ y_2(0) = 0;\ y_3(0) = u \tag{1.5}$$

This solution can agree with the original BV P for a suitable value of u. This means that $y_2(\infty)$ is a function of u; that is

$$\begin{aligned} y_2(\infty) &= \theta(u) \\ r(u) &= \theta(u) - 1 = 0 \end{aligned} \tag{1.6}$$

where $r(u)$ is the boundary residual (the difference between the computed and specified

boundary value). Now Newton method can be used to determine the desired value of u such that the corresponding boundary condition is satisfied.

1.7 Thesis Layout

The thesis is divided into 5 chapters followed by the references section. The details of each chapter are as follows:

- Chapter 1 present a basic introduction to Newtonian and Non-newtonian fluids, their applications, related research, missing links in research, and solutions method of corresponding governing equations.
- Chapter 2 provides a brief overview of the Cross fluid model which is the main focus of this research.
- Chapter 3 presents the modeling of Cross fluid in 2D and its numerical solution using the initial value problem solver technique. The chapter concludes with key observations of the study followed by results in both quantitative and qualitative means.
- Chapter 4 presents the modeling of Cross fluid in 3D with rotational effects and its numerical solution using the initial value problem solver technique. The chapter concludes with key observations of the study followed by results in both quantitative and qualitative means.
- Chapter 5 presents a summary of research followed by future work recommendations

.

Chapter 2
Cross Fluid Model

2.1 Rheology Model

Mostly Non-Newtonian models are enough to investigate a shear thinning and shear thinking region. Notwithstanding the ample application of process engineering, the main limitation of the power-law fluid is that it cannot characterize the liquid behavior at very low and very high shear regions, but only for a restricted shear rate range called the power-law area. To overcome all these limitations cross introduced a model. Which able to predict the flow behavior in the power-law region as well as very high and very low shear regions. Unlike the power-law model, in the cross fluid configuration the shear factor exceeds zero, we attain a finite viscosity, and secondly, it includes a time constant, which makes it good enough for many engineering calculations. The cross-rheology model is a fusion of polymeric solutions a blood-aqueous polymer latex solution. The cross rheology model equation is given below[50].

$$\mu^* = \mu_\infty + (\mu_0 - \mu_\infty)\left[\frac{1}{1 + (\Gamma\dot{\gamma})^{1-n}}\right] \tag{2.1}$$

Or equivalently

$$\frac{(\mu_0 - \mu^*)}{(\mu^* - \mu_\infty)} = (\Gamma\dot{\gamma})^{1-n} \tag{2.2}$$

Where the limiting viscosities at low and high shear rates are μ_0 and μ_∞ .Where Γ is the material constant. n is the flow behavior index. $\dot{\gamma}$ is the shear rate.

2.2 Special Cases

It is interesting to note that we can attain multiple other common viscosity models such as the power-law model, the Sisko model, and the Bingham model by creating some approximation to the Cross equation.

- First and foremost for $n = 1$ and $\Gamma = 0$ the model reduces to simple Newtonian fluids with a constant dynamic viscosity
- Similarly, when $\mu^* \ll \mu_0$ and $\mu^* \gg \mu_\infty$ the cross model reduces to

$$\mu^* = K_1(\dot{\gamma})^{n-1} \tag{2.3}$$

This is a famous power-law model.

- Furthermore if $\mu^* \ll \mu_0$ then

$$\mu^* = \mu_\infty + K_1(\dot{\gamma})^{n-1} \tag{2.4}$$

Which is the Sisko model.

Several researchers have carried out experimental studies on the Cross model over the previous two centuries. Escudier et al. carried out an experimental study and the results on the fluid flow were presented by fitting the Cross model to the non-Newtonian fluid, especially the Xanthan gum (XG). Xie and Jin[13] studied the Cross Rheology equation in order to assess the free surface flow of non-Newtonian fluids. An experimental method, namely the WC-MPS technique, was used to determine the Cross model's four rheology parameters for the numerical application of the Cross equation.

2.3 Governing Boundary Layer Equations for Cross Fluid Model

The conservation equations of mass, linear momentum, and energy for the flow of an incompressible fluid are

$$\nabla \cdot V = 0 \tag{2.5}$$

$$\rho \frac{\partial V}{\partial t} = \nabla \tau \tag{2.6}$$

$$\rho c_p \frac{dT}{dt} = \tau . L - \nabla q \tag{2.7}$$

Where V is the velocity vector, ρ is the density, τ is the Cauchy stress tensor,T is the fluid temperature, c_p is the specific heat constant, q is the heat flux, L and $\frac{d}{dt}$ are the material derivatives. The Cauchy stress tensor for the fluid is defined as,

$$\tau = -PI + \mu^* A_1 \tag{2.8}$$

Where μ^* is the cross model, P is the pressure, I is the identity tensor, A_1 is the first Rivlin-Ericksen tensor. Whereas

$$A_1 = L + L^T, \qquad L = \nabla V \tag{2.9}$$

$$\text{So } A_1 = \begin{bmatrix} 2u_x & u_y + v_x & u_z + w_x \\ u_y & 2v_y & v_x + w_y \\ w_x + u_x & w_y + v_x & 2w_z \end{bmatrix} \tag{2.10}$$

$$\dot{\gamma} = \sqrt{\frac{1}{2} tr(A_1)^2} \tag{2.11}$$

The infinite shear viscosity η_∞ in Eq (2.1) is taken zero often [50] .Due to this consideration, Eq (2.8) will get the following form.

$$\tau = -PI + \mu_0 \left[\frac{1}{1 + (\Gamma\dot{\gamma})^{1-n}}\right] A_1 \tag{2.12}$$

The important aspect of cross fluid is that when $0 < n < 1$ the fluid will behave a shear thickening while if $n > 1$ the fluid will behave a shear-thinning and additionally if $n = 0$ the flow will reduce to Newtonian flow. Through Cartesian coordinates for two-dimensional flow, we consider the velocity field of the form

$$V = [u(x, y), v(x, y)] \tag{2.13}$$

Where u and v are the $x-$ and $y-$component of the velocity vector. Keeping in view the shear rate Eq (2.11) can be written as

$$\dot{\gamma} = \left[4\left(\frac{\partial u}{\partial x}\right)^2 + \left(\frac{\partial u}{\partial y} + \frac{\partial v}{\partial x}\right)^2\right]^{\frac{1}{2}} \tag{2.14}$$

Putting Eq (2.13) in Eq (2.5) and Eq (2.6) while keeping in mind Eq (2.12) and Eq (2.14) a straight forward calculation gets the following form.

$$\frac{\partial u}{\partial x} + \frac{\partial v}{\partial y} = 0 \tag{2.15}$$

$$\rho\left(u\frac{\partial u}{\partial x} + v\frac{\partial u}{\partial y}\right)$$

$$= -\frac{\partial p}{\partial x} + 2\mu_0 \frac{\partial}{\partial x}\left(\frac{\frac{\partial u}{\partial x}}{1 + \left\{\Gamma^2\left(4\left(\frac{\partial u}{\partial x}\right)^2 + \left(\frac{\partial u}{\partial x} + \frac{\partial v}{\partial y}\right)^2\right)\right\}^{\frac{1-n}{2}}}\right) \tag{2.16}$$

$$+ \mu_0 \frac{\partial}{\partial y}\left[\frac{\left(\frac{\partial u}{\partial y} + \frac{\partial v}{\partial x}\right)}{1 + \left\{\Gamma^2\left(4\left(\frac{\partial u}{\partial x}\right)^2 + \left(\frac{\partial u}{\partial y} + \frac{\partial v}{\partial x}\right)^2\right)\right\}^{\frac{1-n}{2}}}\right]$$

$$\rho\left(u\frac{\partial v}{\partial x}+v\frac{\partial v}{\partial y}\right)$$

$$=-\frac{\partial p}{\partial y}+\mu_0\frac{\partial}{\partial x}\left(\frac{\left(\frac{\partial u}{\partial y}+\frac{\partial v}{\partial x}\right)}{1+\left\{\Gamma^2\left(4\left(\frac{\partial u}{\partial x}\right)^2+\left(\frac{\partial u}{\partial x}+\frac{\partial v}{\partial y}\right)^2\right)\right\}^{\frac{1-n}{2}}}\right) \tag{2.17}$$

$$+\mu_0\frac{\partial}{\partial y}\left[\frac{\left(\frac{\partial u}{\partial y}+\frac{\partial v}{\partial x}\right)}{1+\left\{\Gamma^2\left(4\left(\frac{\partial u}{\partial x}\right)^2+\left(\frac{\partial u}{\partial y}+\frac{\partial v}{\partial x}\right)^2\right)\right\}^{\frac{1-n}{2}}}\right]$$

keeping in view the boundary layer analysis one can finally get the following form for the above equations.

$$\frac{\partial u}{\partial x}+\frac{\partial u}{\partial y}=0 \tag{2.18}$$

$$u\frac{\partial u}{\partial x}+v\frac{\partial u}{\partial y}=-\frac{1}{\rho}\frac{\partial p}{\partial x}+\nu\frac{\partial}{\partial y}\left[\frac{\frac{\partial u}{\partial y}}{1+\left\{\Gamma\left(\frac{\partial u}{\partial y}\right)\right\}^{1-n}}\right] \tag{2.19}$$

2.4 Important Non-Dimensional Numbers

Some important parameters that arise during the numerical solution of the non-dimensional boundary layer equations of the Cross fluid are Weissenberg number, Nusselt number, and skin friction coefficient.

2.4 1Weissenberg Number

The Weissenberg number $W_e$originates from Karl Weissenberg, who worked in the field of non-Newtonian fluid. In a non-Newtonian fluid, the stress and strain rate are not linearly related. Non-Newtonian fluids are elastic viscous, which means they combine elastic properties with viscous properties. In a fluid flow when the time-scale is much less than an elastic viscous material's relaxation time, elastic impacts dominate. While on the other hand, when the fluid flow time is much higher than the relaxation time, elastic effects are enough for viscous effects to overcome. The viscous forces-elastic forces ratio is a dimensionless number of special connotations

in the study of non-Newtonian fluid flow depending upon the situations. This is a Weissenberg number:

$$We = \frac{elastic\ froces}{viscous\ forces} \tag{2.20}$$

2.4.2 Skin Friction Coefficient

The ratio of shear stress at the boundary and the dynamic pressure of the free stream is known as the skin friction coefficient

$$C_f = \frac{\tau_w}{\frac{1}{2}\rho v^2} \tag{2.21}$$

Here τ_w is shear stress at the boundary, v is the free stream velocity. For a particular type of flow, C_f depicts the magnitude of the frictional force being felt by the fluid as it moves over the boundary.

2.4.3 Nusselt Number

A Nusselt number is a dimensionless term used to interpret convective heat transfer. Actually, it is the calculation of the ratio between convection heat transfer and conduction heat transfer. Mathematically

$$Nu_x = \frac{Convective\ Heat\ Transfer}{Conductive\ Heat\ Transfer} = \frac{h}{k/x} \tag{2.22}$$

Where "h" is the convective heat transfer coefficient, "x" is the distance from the boundary, and "k" is the thermal conductivity of the fluid. Different values of the Nusselt number represent different flows. For example, Nusselt number "1" represents heat transfer utilizing pure conduction. Whereas values between "1" to "10" are observed for Laminar flows. In this thesis, we will observe values in the range of "1" to "10" (i.e. laminar flows).

Chapter 3

Cross Fluid Flow over a Moving Flat Plate

The present chapter is a pioneering attempt to introduce the boundary layer equations for the two-dimensional flow and heat transfer of the Cross fluid over a moving plate. The system of partial differential equations is converted into highly non-linear ordinary differential equations by introducing appropriate similarity transformations. The solutions of moving flat plates are provided for the shear-thinning as well as the shear-thickening process using a computational procedure namely the bvp4c system and graphs are built. The impact on the velocity and temperature fields of the evolving parameters, namely the power-law index n, the local Weissenberg number We, and the Prandtl number Pr, is investigated through graphs.

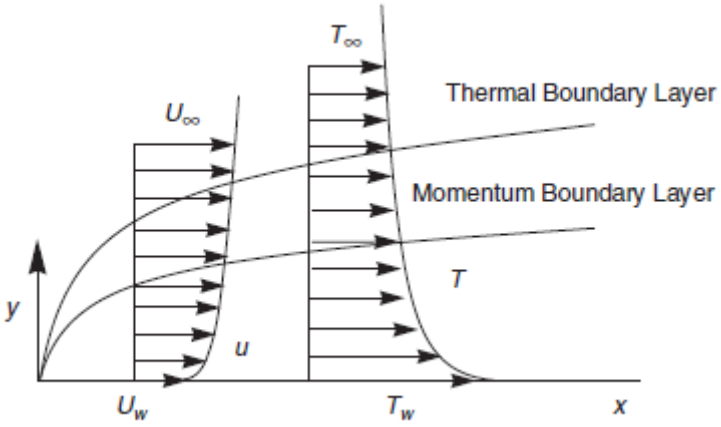

Fig 3.1: Physical sketch of the problem

3.1 Problem Formulation

Consider an incompressible two-dimensional flow and heat transfer of the cross fluid over a moving flat plate. The plate (located at y=0) moving outside the boundary layer with the constant velocity U_w and U_∞ be the fluid velocity. A study on the analysis of heat transfer is carried out due to nonlinear thermal radiation. Moreover, the combined effects of Joule heating and viscous dissipation are considered. The plate is

held at constant $T_w$temperature, while T_∞ implicitly denotes the temperature of the ambient liquid.

$$\frac{\partial u}{\partial x}+\frac{\partial v}{\partial y}=0 \tag{3.1}$$

$$u\frac{\partial u}{\partial x}+v\frac{\partial u}{\partial y}=\nu\ \frac{\partial}{\partial y}\left[\frac{\frac{\partial u}{\partial y}}{1+\left\{\Gamma\left(\frac{\partial \mathrm{u}}{\partial \mathrm{y}}\right)\right\}^{1-n}}\right] \quad Uw<U_\infty \tag{3.2}$$

$$u\frac{\partial u}{\partial x}+v\frac{\partial u}{\partial y}=-\nu\ \frac{\partial}{\partial y}\left[\frac{-\frac{\partial u}{\partial y}}{1+\left\{\Gamma\left(-\frac{\partial \mathrm{u}}{\partial \mathrm{y}}\right)\right\}^{1-n}}\right] \quad U_w>U_\infty \tag{3.3}$$

$$u\frac{\partial T}{\partial x}+v\frac{\partial T}{\partial y}=\alpha\frac{\partial^2 T}{\partial y^2}-\frac{1}{\rho Cp}\left(\frac{\partial q_\gamma}{\partial y}\right) \tag{3.4}$$

Due to parallel free stream and nonlinear thermal radiation the following boundary conditions are produced.

$$u=U_w,\qquad v=0,\ \ T=T_w \text{ at } y=0 \tag{3.5}$$

$$u\to U_\infty,\qquad T\to T_\infty \text{as } y\to\infty \tag{3.6}$$

where $x-$ and $y-$ are the coordinates along and normal to the plate respectively.u and v are the velocity components along the $x-$ and $y-$directions respectively, ν is the kinematic viscosity T is the fluid's temperature, α is the thermal diffusivity, C_p is the specific heat at constant pressure and q_r is the radiative heat flux.

The radiative heat flux qr is given by the Rosseland (1931) approximation as:

$$q_r=-\frac{4\sigma^*}{3k^*}\frac{\partial T^4}{\partial y} \tag{3.8}$$

This is further simplified

$$q_r=-\frac{16\sigma^*}{3k^*}T^3\frac{\partial T}{\partial y} \tag{3.9}$$

So Eq (3.4) will get the final form

$$u\frac{\partial T}{\partial x}+v\frac{\partial T}{\partial y}=\frac{\partial}{\partial y}\left[\left(\alpha+\frac{16\alpha^*T^3}{3\rho C_p k^*}\right)\frac{\partial T}{\partial y}\right] \tag{3.10}$$

Where σ* and k* are the Stefan-Boltzman constant and the mean absorption coefficient.

Now introduce the corresponding similarity transformation for the Eq (3.2-3.4).

$$\eta=y\sqrt{\frac{U}{2\nu x}},u=Uf'(\eta),v=\sqrt{\frac{U\nu}{2x}}(\eta f'-f),\theta(\eta)=\frac{T-T_\infty}{T_w-T_\infty} \tag{3.11}$$

Where $f(\eta)$ represent the dimensionless stream function and $\theta(\eta)$ represent the non-dimensional temperature. The required continuity Eq-(3.1) is satisfied while Eq-(3.2), Eq-(3.3) and Eq-(3.4) with boundary conditions Eq-(3.5) and Eq-(3.6) are transformed into the following form.

$$f'''[1+sign(\gamma-0.5)(1-n)(Wef'')^n]+ff''[1+(Wef'')^n]^2=0 \tag{3.12}$$

$$\theta''[1+Rd(1+(\theta w-1)\theta)^3]+3Rd\left[(1+(\theta w-1)\theta)^2(\theta w-1)\theta'^2\right] + Prf\theta'=0 \tag{3.13}$$

$$f(0)=0, f'(0)=1-\gamma, \theta(0)=1, \quad f'(\infty)\to\gamma, \qquad \theta(\infty)\to 0 \tag{3.14}$$

Where $\gamma=\frac{U_\infty}{U}$ is the velocity ratio parameter, $We=\frac{U\Gamma R_e^{\frac{1}{2}}}{x\sqrt{2}}$ is the Weissenberg number, $Pr=\frac{\nu}{\alpha}$ is the Prandtl number , $Rd=\frac{16\alpha T_\infty^3}{3KK^*}$ are the radiation parameter and $\theta w=\frac{T_w}{T_\infty}$ is the temperature ratio parameter.

The expression provided for the local skin friction coefficient and the local number Nusselt are:

$$C_f=\frac{\tau_w}{\frac{1}{2}\rho U^2}, \qquad N_u=\frac{xq_w}{k(T_w-T_\infty)} \tag{3.15}$$

Where τ_w is local wall shear stress and q_w is described as surface heat flux:

$$\tau_w=\tau_{xy|_{y=0}}=\left[\eta_0\frac{\frac{\partial u}{\partial y}}{1+\left\{\Gamma\left(\frac{\partial u}{\partial y}\right)\right\}^{1-n}}\right]_{y=o}, \qquad q_w=-k\frac{\partial T}{\partial y}|_{y=0} \tag{3.16}$$

In the illumination of the Eq. (3.11) we obtain dimensional forms of the local skin friction coefficient and the local Nusselt number as:

$$\frac{1}{2}Re^{\frac{1}{2}}C_{fx}=\frac{f''(0)}{1+\left(Wef''(0)\right)^{1-n}}, \qquad -Re^{-\frac{1}{2}}Nu_x=[1+Rd\{1+(\theta w-1)\theta\}^3]\theta'(0) \tag{3.17}$$

3.2 Numerical Solution

In order to solve the higher-order differential problems numerically. They are converted into a system of 1st order equations using new variables. Therefore, let $y_1=$

$f; y_2 = f'; \ y_3 = f''; \ y_4 = \theta$ and $y_5 = \theta'$. The equivalent first-order equations are as follows:

$$y_1' = y_2; y_2' = y_3; \tag{3.19}$$

$$y_3' = \frac{-y_1 y_3 [1 + (We y_3)^n]^2}{[1 + \text{sign}(\gamma - 0.5)(1 - n)(We y_3)^n]}; \tag{3.20}$$

$$y_4' = y_5; \tag{3.21}$$

$$y_5' = \frac{-Pr y_1 y_5 - 3Rd[(1 + (\theta w - 1)y_4)^2(\theta w - 1)y_5^2]}{[1 + Rd(1 + (\theta w - 1)y_4)^3]} \tag{3.22}$$

with boundary conditions

$$y_1(0) = 0; \ y_2(0) = \ 1 - \gamma; y_4(0) = 1; \ \ y_2(\infty) = \ \gamma; \ \ y_4(\infty) = \ 0 \tag{3.23}$$

The solution of Eq. (3.19-3.23) is obtained using the fifth order Runge-Kutta integration technique with the following initial conditions

$$y_1(0) = \ 0; \ y_2(0) = \ 0; \ y_3(0) = \ u_1; \ \ y_4(0) = \ 1; \ \ y_5(0) = \ u_2 \tag{3.24}$$

This solution can agree with the original BV P for suitable values of u_1 and u_2.

3.3 Results and Discussion

Using Matlab code bvp4c, the boundary value problem given in eq-3.12 and eq-3.13 with boundary conditions eq-3.14 are solved. To make sure that the accuracy of obtained computations and validation of the code we have reproduced the results of [18]. After code validation now we will examine the impact of various evolving parameters on the velocity and temperature flow field. The obtained results are tabulated in Tables 3.1-3.3. Table 3.1 is designed to provide a skin friction coefficient and Table 3.3 provides heat transfer rate numerical values for various values of relevant parameters.

Figure 3.4 indicates the horizontal velocity variation with an improvement in the velocity parameter ratio γ. It is observed that the velocity function f' rises and that the thickness of the boundary layer declines when $0 < \gamma < 0.5$ increases. There is no boundary layer formation at γ=0.5. In this region, the free stream velocity is less than the velocity of the plate. The analysis of the impact of the power-law index $'n'$ on the velocity profile and fluid temperature profile is shown in Fig.3.2 and Fig.3.3 for two different values of γ=0.2 and γ =1. examination of these figures reveals that the velocity profiles along with the momentum boundary layer thickness show a growing trend for both($\gamma < 0.2$ and $\gamma > 1$) for increasing the power law of index. The effect

of the power-law index $'n'$ on the temperature profile is observed in fig.3.5. In fig.3.5 the thermal boundary layer reveals a declining tendency while rising the power law of the index. The physical explanation for this behavior is that the fluid is facing less resistance due to low viscosity which causes the velocity of the fluid to rise and decrease in temperature of the fluid.

Figures 3.6 and 3.7 show the behavior of the velocity profiles and temperature profile corresponding to a change in Weissenberg's local number. The study of the figures(3.6-3.7) reveals that We trigger the velocity of the fluid to increase and decaying in the temperature of the fluid. Physically, an enhancement in the Weissenberg number value We causes the velocity of the fluid to boost and the temperature of the fluid to decrease.

Fig. 3.8 Displays the effect on the temperature profile of the Prandtl number Pr for fixed n and We values. Prandtl number is the resultant of viscosity, Specific heat, and thermal conductivity. Furthermore, Pr regulates the relative velocity thickness and the thermal boundary layers. Keeping in view all the above aspects that smaller Prandtl liquids lead to speedier heat diffusion in thicker thermal boundaries as compared to larger Prandtl liquids in thinner boundaries. Thus the rise in Pr leads to a decrease in the thermal boundary layer thickness and an improvement in the heat transfer rate at the plate. Perhaps it can be guaranteed that the Prandtl number can be used to upgrade the cooling rate in the conductive liquid flow. The influence of temperature ratio θ_w on temperature is shown in fig.3.9. The higher temperature ratio parameter θ_w indicates a higher plate temperature compared to ambient temperature. Due to which the temperature of the fluid rises because of the hotter surface. Figure 3.10 shows that, regardless of the range of values chosen for the velocity ratio γ.

3.4 Concluding Remarks

This study is seminal work in the development of cross fluid flow boundary layer equations. Modeled partial differential equations of cross fluid were Simplified by implementing appropriate similarity transformations and numerical solutions using the bvp4c scheme. The key conclusions can be summarized as:

- The increasing power-law index values culminated in the velocity of fluid elevation while a decrease in the thermal boundary layer was observed.

- The velocity profiles reach the free stream velocity at a long distance from the plate suggesting a rise in the momentum boundary layer thickness with an increase in the velocity ratio γ. An increase in the temperature and heat transfer rate from the plate occurred.
- The momentum boundary layer and Velocity fields are demonstrated the elevation impact of the growing local Weissenberg number. The contrary phenomenon for the thermal boundary layer was found.
- The Prandtl number's elevated values reduced the temperature profile as well as the thickness of the thermal boundary layer.
- The temperature rises in the region and from the plate the heat flux reduces as θw is increasing.

Table 3.1: Numerical validation for Newtonian Fluid Case

γ	Cortell [18]	Present
0	−0.627547	−0.627555
0.2	−0.363308	−0.363336
0.4	−0.115777	−0.115809
0.6	0.109652	0.109638
0.8	0.307378	0.307354
1	0.469602	0.469600

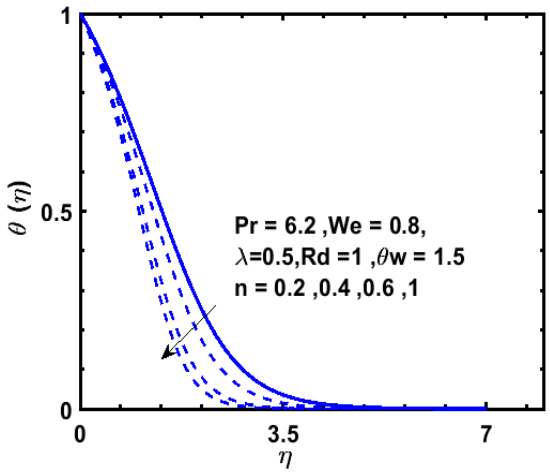

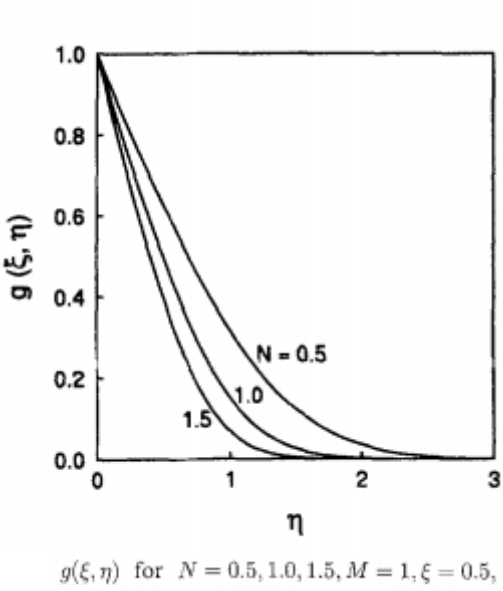

$g(\xi, \eta)$ for $N = 0.5, 1.0, 1.5, M = 1, \xi = 0.5,$

Table 3.2: Numerical findings Local skin friction for various values of, n and We.

γ	n	We	$f''(0)$
0	0.6	0.8	- 0.443939
0.2			- 0.295422
0.4			- 0.106581
0.6			0.124278
0.8			0.385465
1			0.625574
0.2	0.1	0.2	- 0.87292
	0.3		- 0.439217
	0.5		- 0.350406
	1.2		- 0.357323
1	0		0.664115
	0.5		0.55066
	1		0.496975
	2		0.472321
0.3	0.8	0.5	- 0.213935
		1	- 0.197768
		1.5	- 0.184016
		2	- 0.171461

Table 3.3: Numerical findings for Local Nusselt number against different values of *n*, We, θw,γ,Rd, Pr.

Pr	γ	n	We	θw	Rd	$\theta'(0)$
6.2	0.3	0.2	0.8	1.5	1	- 0.610192
		0.5				- 0.642717
		0.8				- 0.644514
		1.2				- 0.640061
	0	0.8				- 0.738588
	0.3					- 0.643104
	0.7					-0.545214
	1					-0.485732
	0.3		0.5			- 0.641106
			1.5			- 0.647132
			2.5			- 0.651992
0.7	0.6		0.8			- 0.191498
1						- 0.234596
2						- 0.347346
7						- 0.690414
				1		- 1.37613
				1.2		- 1.18304
				1.6		- 0.842045
				2		- 0.603513

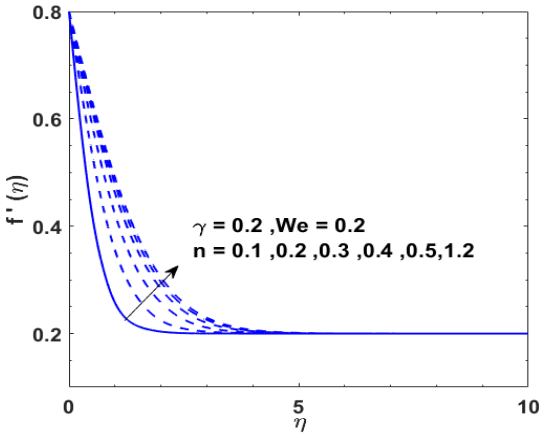

Fig 3.2: Velocity curve f' Variation against η for different values of n for Sakiadis $\gamma = 0$

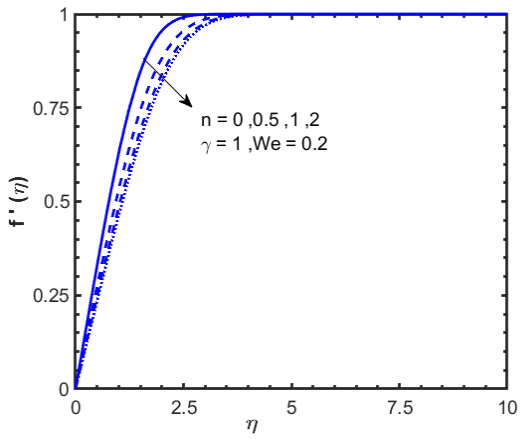

Fig 3.3: Velocity curve f' Variation against η for different values of n for Blasius $\gamma = 1$.

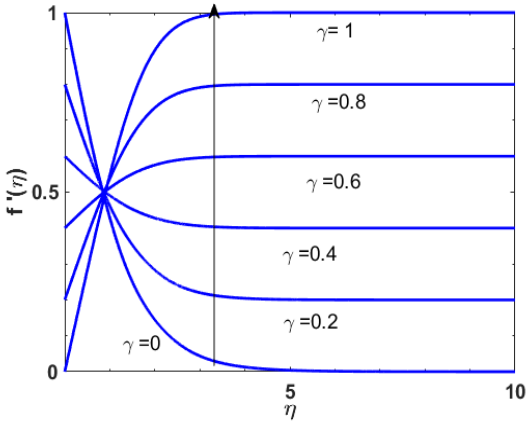

Fig 3.4:. Velocity curve f' Variation against η for different values of γ

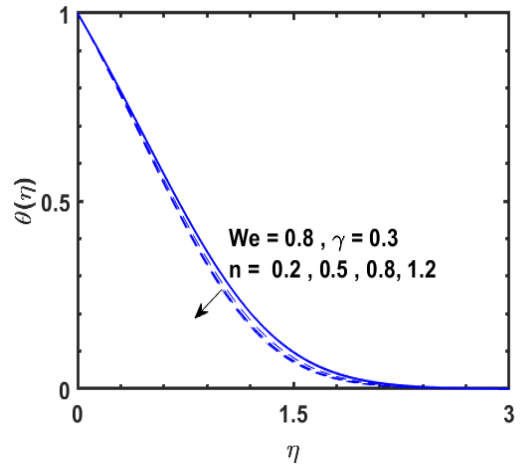

Fig 3.5: Temperature curve θ Variation against η for different values of n.

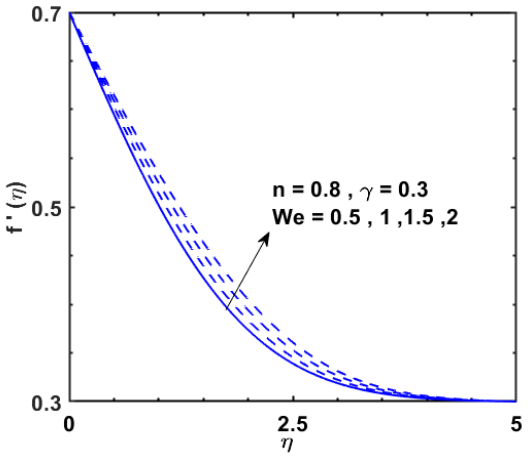

Fig 3.6: Velocity curve f' Variation against η for different values of We.

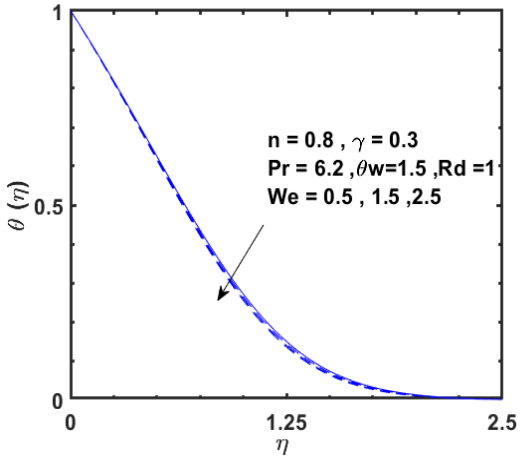

Fig 3.7: Temperature curve θ Variation against η for different values of We.

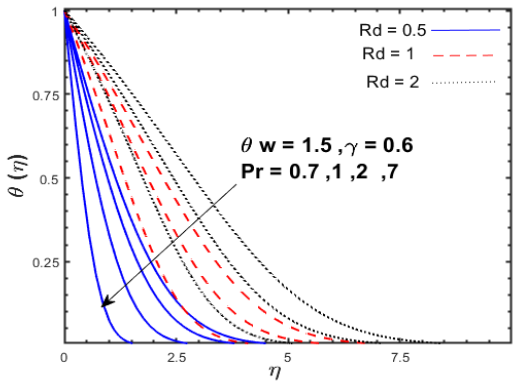

Fig 3.8: Temperature curve θ Variation against η for different values of Pr.

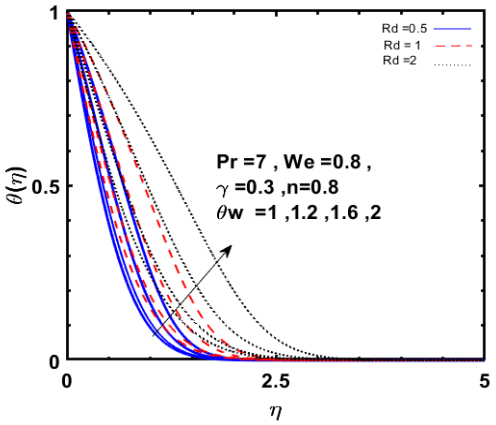

Fig 3.9: Temperature curve θ Variation against η for different values of θw .

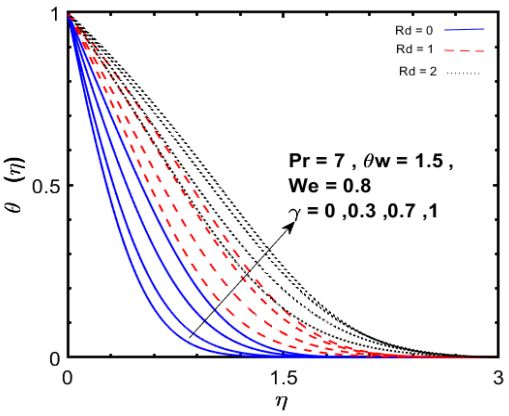

Fig 3.10: Temperature curve θ Variation against η for different values of γ.

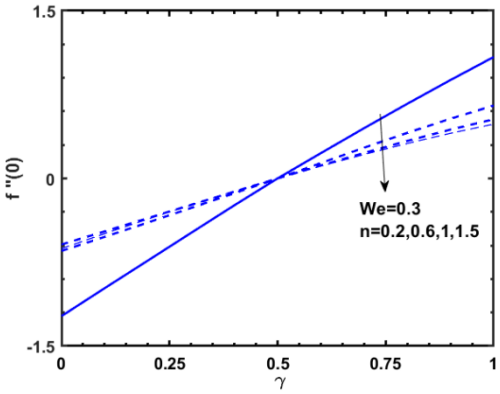

Fig 3.11: $f''(0)$ Variation against η for different values of n.

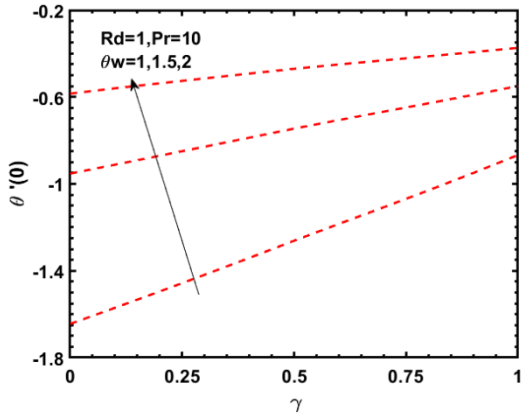

Fig 3.12: $\theta'(0)$ Variation against η for different values of θw

Chapter 4

3D Rotating Flow of Cross Fluid over a Stretching Sheet

In this chapter, a description of the Cross fluid's rotating flow and heat transfer over a radially stretching surface is established. The present study gives the Cross fluid with 3-d boundary layer equations. Through introducing appropriate similarity transformations, the derived momentum and energy equations are further transformed into nonlinear ordinary differential equations. The equation model is then solved numerically, using the bvp4c computational technique. For certain parameter values such as the power-law series the local Weissenberg number and the Prandtl number, velocity, and temperature profiles are established. In comparison, for several physical parameters, the numerical values for the local skin friction coefficient and the local number Nusselt are tabled.

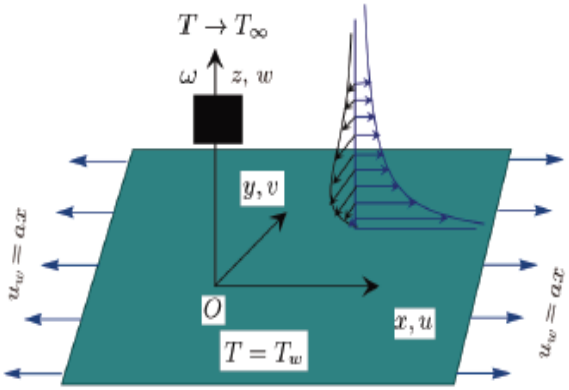

Fig 4.1: Physical configuration and coordinate system

4.1 Problem Formulation

Assuming a steady, laminar, and incompressible cross fluid flow induced by a stretch sheet in a rotating flow. Let (u, v, w) be the components of the velocity vector in the direction of the Cartesian axes (x, y, z) with the axes rotating at an angular velocity Ω in the direction of z with a constant temperature T_w whereas T_∞ indicates the ambient

fluid temperature. The governing equations derived for the rotating flow cross model are below using the standard the boundary layer approximation.

$$\frac{\partial u}{\partial x}+\frac{\partial v}{\partial y}+\frac{\partial w}{\partial z}=0 \tag{4.1}$$

$$u\frac{\partial u}{\partial x}+v\frac{\partial u}{\partial y}+w\frac{\partial u}{\partial z}-2\Omega v=\upsilon\frac{\partial}{\partial z}\left[\frac{\frac{\partial u}{\partial z}}{1+\left\{\Gamma\left(\frac{\partial u}{\partial z}\right)\right\}^{1-n}}\right] \tag{4.2}$$

$$u\frac{\partial v}{\partial x}+v\frac{\partial v}{\partial y}+w\frac{\partial v}{\partial z}+2\Omega u=\upsilon\frac{\partial}{\partial z}\left[\frac{\frac{\partial v}{\partial z}}{1+\left\{\Gamma\left(\frac{\partial v}{\partial z}\right)\right\}^{1-n}}\right] \tag{4.3}$$

$$u\frac{\partial T}{\partial x}+v\frac{\partial T}{\partial y}+w\frac{\partial T}{\partial z}=\alpha\frac{\partial T^2}{\partial z^2}+\frac{1}{\rho C_p}\left(\frac{\partial q_r}{\partial z}\right) \tag{4.4}$$

u,v,w are the velocity components respectively, n is the power-law index behavior, Ω is the angular velocity. ν the kinematic viscosity, Γ is cross-time constant, T the fluid temperature, α the thermal diffusivity, C_p the specific heat at constant pressure and q_r is the radiative heat flux in the above equation. With the corresponding boundary conditions

$$\begin{gathered}u=u_w=ax,\quad v=0\ ,w=0\ ,\ T=T_w\ ,\quad at\quad z=0\\ u=0\ ,\quad v=0\quad ,\quad T=T_\infty\qquad as\ z\to\infty\end{gathered} \tag{4.5}$$

The Rosseland (1931) approximation provides the radiative heat flux qr as:

$$q_r=-\frac{4\sigma^*}{3k^*}\frac{\partial T^4}{\partial y} \tag{4.6}$$

Which is further simplified as

$$q_r=-\frac{16\sigma^*}{3k^*}T^3\frac{\partial T}{\partial y} \tag{4.7}$$

So Eq-(4.7) will get the final form

$$u\frac{\partial T}{\partial x}+v\frac{\partial T}{\partial y}+w\frac{\partial T}{\partial z}=\frac{\partial}{\partial z}\left[\left(\alpha+\frac{16\alpha^*T^3}{3\rho C_p k^*}\right)\frac{\partial T}{\partial z}\right] \tag{4.8}$$

where σ* is the Stefan-Boltzman constant and k* is the mean absorption coefficient. The similarity transformations of equations (4.1) – (4.4) are.

$$\eta=\sqrt{\frac{a}{\upsilon}}z\quad ,\quad u=axf'(\eta)\quad ,\quad v=axg(\eta)\quad , \tag{4.9}$$

$$w = -\sqrt{av}f(\eta), \qquad \theta(\eta) = \frac{T - T_\infty}{T_w - T_\infty}$$

Eq-(4.1) is therefore automatically fulfilled whereas Eq-(4.2), (4.3), and (4.5) are applied to the form below.

$$f'''(1 + (1-n)(Wef'')^n) - \left[\left(f'^2 - ff'' - 2\lambda g\right)(1 + (Wef'')^n)^2\right] = 0 \tag{4.10}$$

$$g''(1 + (1-n)(Weg')^n) - [(f'g - fg' + 2\lambda f')(1 + (Weg')^n)^2] = 0 \tag{4.11}$$

$$\theta''[1 + Rd(1 + (\theta w - 1)\theta)^3] + 3Rd\left[(1 + (\theta w - 1)\theta)^2(\theta w - 1)\theta'^2\right] + Prf\theta' = 0 \tag{4.12}$$

$$f(0) = 0, \quad f'(0) = 1, \qquad g(0) = 0, \qquad \theta(0) = 1$$
$$f'(\infty) = 0, \quad g(\infty) = 0, \quad \theta(\infty) = 0 \tag{4.13}$$

In which $Pr = \frac{\upsilon}{\alpha}$ is the Prandtl number. $Rd = \frac{16\alpha T_\infty^3}{3KK^*}$ is the radiation parameter, $\lambda = \frac{\Omega}{a}$ is the ratio of rotation rate to the stretching rate, $We = \Gamma ax\sqrt{\frac{a}{\upsilon}}$ is the local Weissenberg number, $\theta w = \frac{T_w}{T_\infty}$ is the temperature ratio parameter.

The concepts of local skin friction and heat transmission rate are

$$C_{fx} = \frac{\tau_{xz}}{\rho_f {U_w}^2} C_{fy} = \frac{\tau_{yz}}{\rho_f {U_w}^2}$$
$$N_{ux} = \frac{xq_w}{k_f(T_w - T_\infty)} \tag{4.14}$$

Where

$$\tau_{xz} = \eta_{nf}\frac{\partial u}{\partial z}|_{z=0}, \qquad \tau_{yz} = \eta_{nf}\frac{\partial v}{\partial z}|_{z=0},$$
$$q_w = -k_{nf}\frac{\partial T}{\partial z}|_{z=0} + q_r|_{z=0} \tag{4.15}$$

Using Eq-(4.9) in Eq-(4.14) one can obtain the following dimensionless form

$$C_{fx}Re^{\frac{1}{2}} = \frac{2f''(0)}{[1 + (Wef''(0)]^n}, \qquad C_{fy}Re^{\frac{1}{2}} = \frac{2g'(0)}{[1 + (Weg'(0)]^n} \tag{4.16}$$

$$N_{ux}{R_{ex}}^{-\frac{1}{2}} = -[1 + Rd\{1 + (\theta w - 1)\theta\}^3]\theta'(0) \tag{4.17}$$

Numerical solutions of Eq-(4.10-4.12) are computed using a computational technique bvp4c.

4.2 Numerical Solution

In order to solve the higher-order differential problems numerically. They are converted into a system of 1st order equations using new variables. Therefore, let $y_1 = f; y_2 = f'; \ y_3 = f''; \ y_4 = g; \ \ y_5 = g'; \ \ y_6 = \theta$ and $y_7 = \theta'$. The equivalent first-order equations are as follows:

$$y_1' = y_2; y_2' = y_3; \tag{4.18}$$

$$y_3' = \frac{[(y_2^2 - y_1 y_3 - 2\lambda y_4)(1 + (We y_3)^n)^2]}{1 + (1-n)(We y_3)^n}; \tag{4.19}$$

$$y_4' = y_5 \ ; \tag{4.20}$$

$$y_5' = \frac{[(y_2 y_4 - y_1 y_5 + 2\lambda y_2)(1 + (We y_5)^n)^2]}{1 + (1-n)(We y_5)^n} \tag{4.21}$$

$$y_6' = y_7; \tag{4.22}$$

$$y_7' = \frac{-Pr y_1 y_7 - 3Rd[(1 + (\theta w - 1)y_6)^2(\theta w - 1)y_7^2]}{[1 + Rd(1 + (\theta w - 1)y_6)^3]} \tag{4.23}$$

with boundary conditions

$$\begin{gathered} y_1(0) = 0; \ y_2(0) = \ 1; y_4(0) = 0; \ y_6(0) = 1; \\ y_2(\infty) = 0; \ \ y_4(\infty) = \ 0; \ \ y_6(\infty) = \ 0 \end{gathered} \tag{4.24}$$

The solution of Eq. (4.18-4.23) is obtained using the fifth order Runge-Kutta integration technique with the following initial conditions

$$\begin{gathered} y_1(0) = \ 0; \ y_2(0) = \ 0; \ y_3(0) = \ u_1; \\ y_4(0) = \ 0; \ \ y_5(0) = \ u_2; \ y_6(0) = \ 1; \ \ y_7(0) = \ u_3 \end{gathered} \tag{4.25}$$

This solution can agree with the original BV P for suitable values of $u_1; u_2$ and u_3.

4.3 Results and Discussion

The estimated results for the local skin frictions $f''(0)$ and $g'(0)$ and the local Nusselt number is tabulated below Table 4.1-4.3. Figures 4.2 and 4.3 describe the results of power-law index n on the dimensionless velocity components x− and y− respectively. As the value of the power-law of index n enlarges the flow accelerates in both x and y directions. Fig's review. 4.2-4.3 shows a growing trend in the velocity profiles along with the boundary layer thickness. The practical explanation for this phenomenon is that due to low viscosity, fluid experiences less pressure, The impact

of the λ ratio on the velocity components x− and y− respectively are explained in Fig.4.4 and 4.5. Larger λ values suggest reduced stretching rates (along the x-direction) relative to the rate of rotation. Just because of that, the x− component of velocity $f'(\eta)$ is inversely proportional to the rotation ratio parameter λ and the magnitude of the y− component of velocity $g(\eta)$ increases with an increase in λwhich triggers a rise in fluid velocity. Fig-4.6 and 4.7 depict the Weissenberg number We dependency on the fluid velocity profiles $f'(\eta)$ and (η) . The examination of these figures demonstrates that we boost the fluid velocity. Fig. 4.6-4.7 shows an increment in the thickness of the momentum boundary layers of $f'(\eta)$ and $g(\eta)$ with increasing values of the Weissenberg number We.The impact of the λ rotation ratio parameter on the temperature of fluid $\theta(\eta)$is shown in Fig-4.8. Due to variation in λ rise in temperature and boundary layer thickness occurs and the influence is felt prominently. The decrease in the temperature profile, as well as the thermal boundary thickness corresponding to the enhancement in the power-law index n, are shown in Fig-4.9. Fig-4.10 illustrates the reliance of the Weissenberg number We on the temperature of the fluid. Examination of this figure conveys the rise in We lead to a reduction in the temperature of fluid and decreases in the thermal boundary structure. The physical explanation for this action is that fluid experiences less pressure because of the reduced viscosity due to which the fluid temperature decreases. Temperature profiles are sketched in Figure 4.11 for several values of the temperature ratio parameter θ_w for different radiation parameters. Profiles shift from normal shape to thicker profiles when the θ_w is increased. The greater temperature ratio parameter in the plate suggests a higher temperature than the ambient temperature. This is a broader variation between the wall temperature and the ambient which eventually transmits a thicker thermal border layer. Fig-4.12 demonstrates how the Prandtl number Pr influences the temperature of fluid $\theta(\eta)$. The enhanced Prandtl numbers lead to a lower temperature distribution and thermal boundary thickness. The Prandtl number physically indicates the ratio of the momentum diffusivity to the thermal diffusivity. The thermal diffusivity becomes weaker for elevated Pr-values as a result of which the heat flow into the fluid is restricted and thermal boundary layer structures are diminished. Due to high thermal conductivity, heat diffuses quicker from the wall for fluids with small Prandtl numbers. Therefore, the Prandtl number serves as a limiting factor in the conduction of flows to regulate the cooling

intensity.Figs-4.13-14 illustrate the influence of local Nusselt number vs Radiation parameter R_d for different values of θ_w .From the We see a significant increase in the rate of heat transfer when θ_w is increased.

4.4 Concluding Remarks

A cross rotating fluid model is studied for flow and heat transfer over a stretching sheet. The current study shows the boundary layer flow and thermal transmission of cross fluid over a radially stretching sheet in rotating behavior. Using suitable local similarity transformations, the developed partial differential equations are transformed into ordinary differential equations and implemented numerically with BVP4C. The graphs were designed for the velocity and temperature field that corresponds to the emerging parameters. The summarized key results in this work are:

- The y-velocity component is negative with a parabola distribution.
- The parameter λ, which provides the ratio between the rotating and the stretching rates, has a qualitatively Converse effect on the velocity components x− and y. While temperatures Profiles showed a progressive trend with an increase in λ.
- The f' and g velocity distributions increase when using higher power-law index values parameter n. A decrease in the temperature profile was visualized for increasing power-law index values n number
- The temperature function has an exceptional S-shaped profile indicating the existence of an adiabatic case for the large enough wall to ambient temperature ratio.
- Velocity fields and the structures of the momentum boundary layer demonstrated the same enhancement tendency for the rising Weissenberg number. However, with the growth of the local Weissenberg number values, the thermal boundary layer slowly deteriorated.
- The local Nusselt number is directly proportional to the temperature ratio parameter. It leads to a greater temperature difference between the wall and the ambient as well as a thicker thermal boundary layer.

Table 4.1: Numerical Validation for Newtonian Fluid.

λ	Wang [42]			
	$f''(0)$	$g'(0)$	$f''(0)$	$g'(0)$
0.0	-1.0000	-0.0000	-1.000000	-0.000000
0.5	-1.1384	-0.5128	-1.138381	-0.512760
1.0	-1.3250	-0.8371	-1.325029	-0.837098
2.0	-1.6523	-1.2873	-1.652352	-1.287258
5.0	-2.3901	-2.1506	-2.390141	-2.150562

Table 4.2: Skin-friction coefficients $f''(0)$ and $g'(0)$ numerical values against η for different emerging parameters λ,n, and We.

λ	n	We	$f''(0)$	$g'(0)$
0	0.8	0.8	- 0.631987	0
0.5			- 0.684552	- 0.428399
1			- 0.747729	- 0.603203
1.5			- 0.791617	- 0.697665
2			- 0.817958	- 0.755433
0.5	0	0.8	-1.60991	-0.725151
	0.4		- 1.3297	- 0.550272
	0.6		- 0.877135	- 0.457213
	1		-0.698278	-0.436952
	0.8	0	-1.13838	-0.51276
		1	- 0.61043	- 0.409593
		2	- 0.384142	- 0.30242
		3	- 0.242617	- 0.230158

Table 4.3: Numerical findings of local Nusselt number for different values of embedded parameters

Pr	λ	n	We	θw	Rd	$\theta'(0)$
6.2	0	0.5	0.6	1.5	1	- 0.302885
	0.5					- 0.282938
	1					- 0.255167
	2					- 0.206609
	0.5	0.2	0.8			- 0.24475
		0.4				- 0.266718
		0.6				- 0.299477
		1				-0.313663
		0.6	0.5			- 0.293745
			1			- 0.303147
			1.5			- 0.314212
			2			- 0.354017
0.2						- 0.026140
2						- 0.131361
4						- 0.222372
7						- 0.32303
6.2			0.8	1		- 1.18748
				1.5		- 0.298849
				2		- 0.047025
				3		- 0.029273
				1.5	0	- 1.77942
					0.5	- 0.655601
					1	- 0.299477
					1.5	- 0.162991
					2	- 0.094575

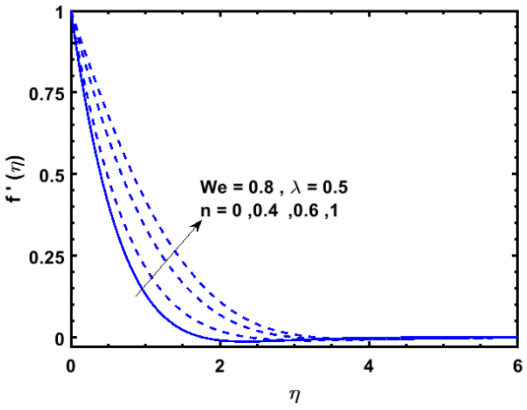

Fig 4.2: The velocity curve $f'(\eta)$ variation against η for various n values.

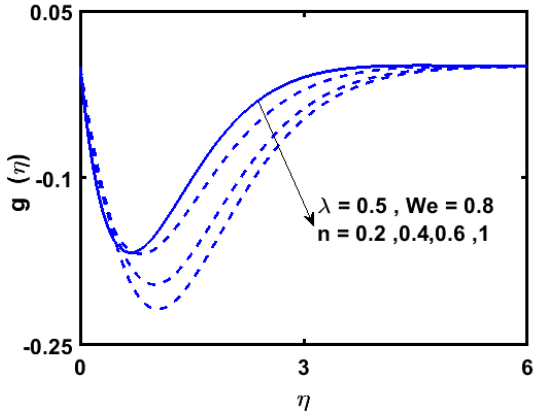

Fig 4.3: The velocity curve $g(\eta)$ variation against η for various n values.

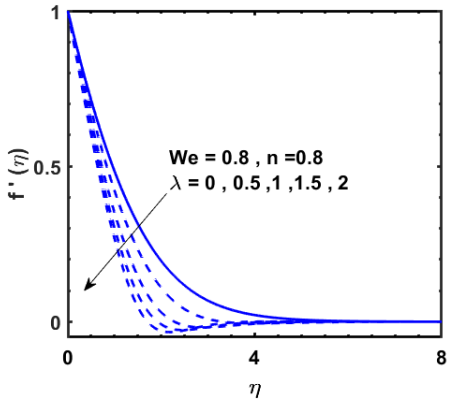

Fig 4.4: Velocity curve $f'(\eta)$ Variation against η for different values of λ.

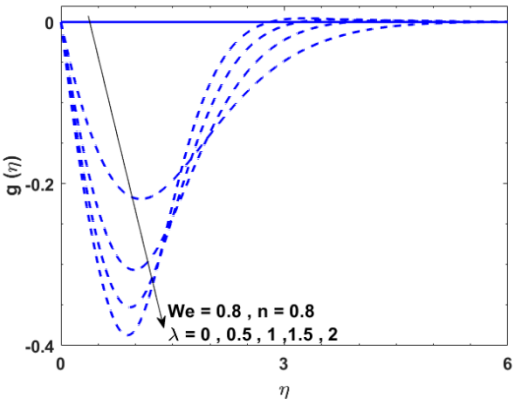

Fig 4.5: Velocity curve $g(\eta)$ Variation against η for different values of λ.

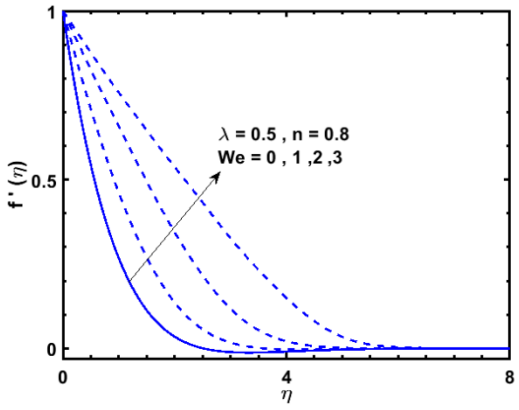

Fig 4.6: Velocity curve $f'(\eta)$ Variation against η for different values of We.

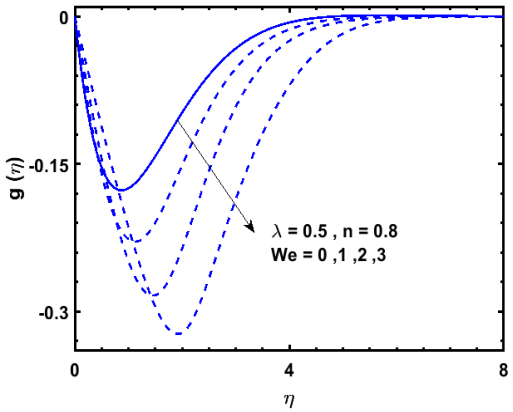

Fig 4.7: Velocity curve $g(\eta)$ Variation against η for different values of We.

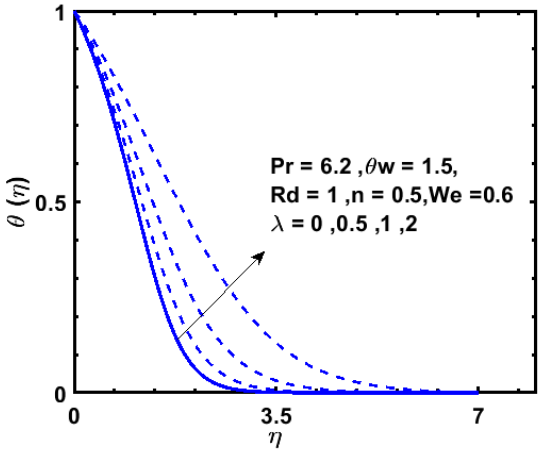

Fig 4.8: Temperature curve θ Variation against η for different values of λ .

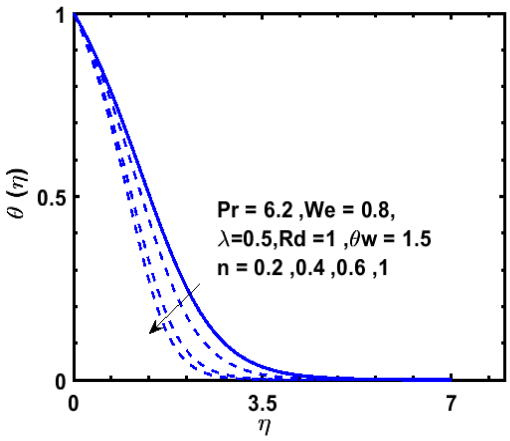

Fig 4.9: Temperature curve θ Variation against η for different values of n .

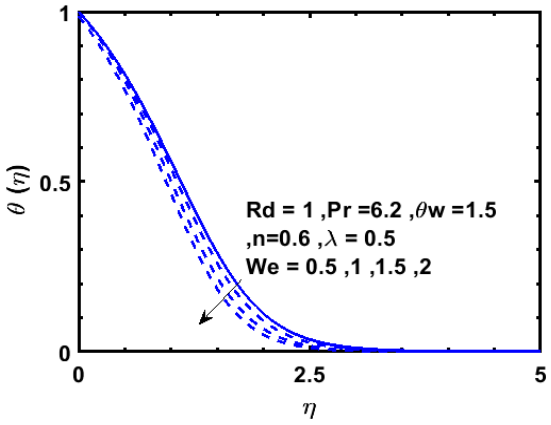

Fig 4.10: Temperature curve θ Variation against η for different values of We .

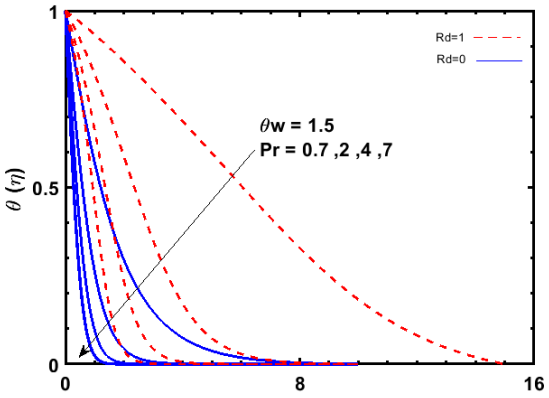

Fig 4.11: Temperature curve θ Variation against η for different values of Pr .

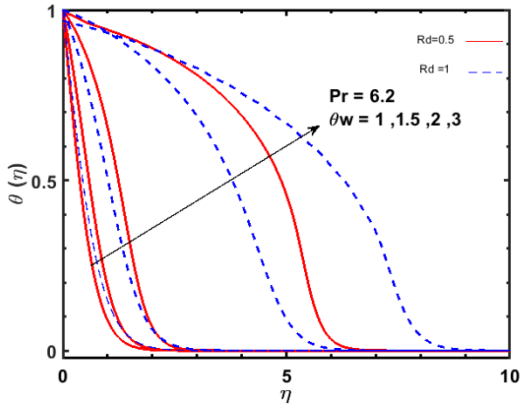

Fig 4.12: Temperature curve θ Variation against η for different values of θw .

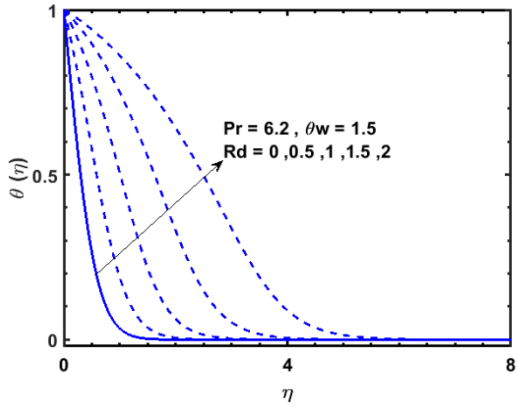

Fig 4.13: Temperature curve θ Variation against η for different values of Rd .

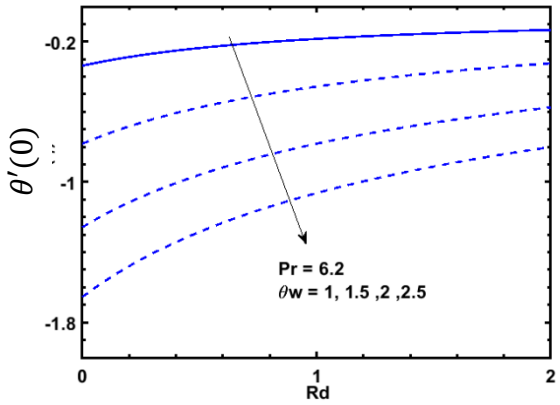

Fig 4.14: Local Nusselt number curve $\theta'(0)$ Variation against Rd for different values of θw.

Chapter 5

Summary and Future Recommendations

5.1 Summary

The key findings of the current work are as follows:

- We have successfully presented the boundary layer equation of Cros fluid for both 2D and 3D flows.
- The non-Newtonian parameters n, We have the same effects in both 2D and 3D flows.
- The rotating and the stretching rates ratio parameter λ showed that temperature BL increases with an increase in λ.
- The temperature BL has S-shaped profiles indicating the existence of an adiabatic case for the large enough wall to ambient temperature ratio.
- The local Nusselt number is directly proportional to the temperature ratio parameter.

5.2 Future Recommendations

The present work can be extended in the following directions:

- Von Karman and Bodewadt flow of Cross fluid
- MHD flow of Cross fluids
- Cross fluid flow in a porous media
- Flow and heat transfer of Cross fluid with nanoparticles.

References

[1]. Steffe, J.F. Rheological Methods in Food Process Engineering, *Freeman Press* (1992)

[2]. Blasius, H. Grenzschichten in Flüssigkeiten mit kleiner Reibung. Zeits. *Math. Phys*, **56**, 1-37 (1908).

[3]. Howarth, L. On the Solution of the Laminar Boundary Layer Equations. *Proceedings of the Royal Society of London. Series A, Mathematical and Physical Sciences* **164** 547–579 (1937).

[4]. Sakiadis, B. C. Boundary-layer behavior on continuous solid surfaces: I. Boundary-layer equations for two-dimensional and axisymmetric flow. *AIChE J.* **7**, 26–28 (1961).

[5]. Sakiadis, B. C. Boundary-layer behavior on continuous solid surfaces: II. The boundary layer on a continuous flat surface. *AIChE J.* **7**, 221–225 (1961).

[6]. Crane, L. J. Flow past a stretching plate. Zeitschrift für Angew. Math. und Phys. *ZAMP* **21**, 645–647 (1970).

[7]. Acrivos, A., Shah, M. J. & Petersen, E. E. Momentum and heat transfer in laminar boundary-layer flows of non-Newtonian fluids past external surfaces. *AIChE J*. **6,** 312–317 (1960).

[8]. Tashtoush, B., Kodah, Z. & Al-Ghasem, A. Heat transfer analysis of a non-Newtonian fluid on a power-law stretched surface with suction or injection for uniform and cooled surface temperature. *Int. J. Numer. Methods Heat Fluid Flow* **10**, 385–396 (2000).

[9]. Schowalter, W. R. The application of boundary-layer theory to power-law pseudoplastic fluids: Similar solutions. *AIChE J.* **6,** 24–28 (1960).

[10]. Eringen, A. Theory of Micropolar Fluids. *Indiana Univ. Math. J.*

16, 1–18 (1966).

[11]. Pakdemirli, M. Boundary layer flow of power-law fluids past arbitrary profiles. *IMA J. Appl. Math*. **50**, 133–148 (1993).

[12]. Hassanien, I. A., Abdullah, A. A. & Gorla, R. S. R. Flow and heat transfer in a power-law fluid over a nonisothermal stretching sheet. *Math. Comput. Model*. **28**, 105–116 (1998).

[13]. Jalil, M., Asghar, S. & Mushtaq, M. Analytical solutions of the boundary layer flow of power-law fluid over a power-law stretching surface. *Commun. Nonlinear Sci. Numer. Simul*. **18**, 1143–1150 (2013).

[14]. Andersson, H. I., Bech, K. H. & Dandapat, B. S. Magnetohydrodynamic flow of a power-law fluid over a stretching sheet. *Int. J. Non. Linear. Mech*. **27**, 929–936 (1992).

[15]. Dunn, J. E. & Fosdick, R. L. Thermodynamics, stability, and boundedness of fluids of complexity 2 and fluids of second grade. *Arch. Ration. Mech. Anal*. **56,** 191–252 (1974).

[16]. Dunn, J. E. & Rajagopal, K. R. Fluids of differential type: Critical review and thermodynamic analysis. *Int. J. Eng. Sci.* **33,** 689–729 (1995).

[17]. Hayat, T. & Khan, M. Homotopy Solutions for a Generalized Second-Grade Fluid Past a Porous Plate. *Nonlinear Dynamics*. **42** (2005).

[18]. Cortell, R. Flow and heat transfer in a moving fluid over a moving flat surface. *Theor. Comput. Fluid Dyn*. **21**, 435–446 (2007).

[19]. Gupta, P. S. & Gupta, A. S. Heat and mass transfer on a stretching sheet with suction or blowing. *The Canadian Journal of Chemical Engineering*. **55** 744–746 (1977).

[20]. Salleh, M. Z., Mohd Rohni, A. & Amin, N. Boundary Layer Flow Due to a Moving Flat Plate in Micropolar Fluid. J. Teknol. 43,

(2005).

[21]. Siekman, J. The laminar boundary layer along a flat plate. *Z. Flugwiss*. **10**, 278–281 (1962).

[22]. Tsou, F. K., Sparrow, E. M. & Goldstein, R. J. Flow and heat transfer in the boundary layer on a continuous moving surface. *Int. J. Heat Mass Transf.* **10**, 219–235 (1967).

[23]. Hayat, T., Iqbal, Z., Qasim, M. & Obaidat, S. Steady flow of an Eyring Powell fluid over a moving surface with convective boundary conditions. *Int. J. Heat Mass Transf.* **55**, 1817–1822 (2012).

[24]. Mustafa, M., Hayat, T., Pop, I. & Aziz, A. Unsteady boundary layer flow of a Casson fluid due to an impulsively started moving flat plate. *Heat Transf. - Asian Res*. **40**, 563–576 (2011).

[25]. Ellahi, R., Alamri, S. Z., Basit, A. & Majeed, A. Effects of MHD and slip on heat transfer boundary layer flow over a moving plate based on specific entropy generation. *J. Taibah Univ. Sci*. **12,** 476–482 (2018).

[26]. Loper, D. E. Steady hydromagnetic boundary layer near a rotating, electrically conducting plate. *Phys. Fluids* **13**, 2999–3002 (1970).

[27]. Debnath, L. On Unsteady Magnetohydrodynamic Boundary Layers in a Rotating Flow. *ZAMM - Zeitschrift für Angew. Math. und Mech*. **52**, 623–626 (1972).

[28]. Gupta, A. S. Ekman layer on a porous plate. *Phys. Fluids* **15**, 930–931 (1972).

[29]. Narasimha Murthy, S. & Prabhakar Ram, R. K. MHD ekman layer on a porous plate. *Nuovo Cim. B Ser*. **11 29**, 296–302 (1975).

[30]. Taylor, G. I. Experiments with rotating fluids. *Proc. R. Soc. London. Ser. A, Contain. Pap. a Math. Phys. Character* **100**, 114–121 (1921).

[31]. Greenspan, H. P.. The theory of rotating fluids. *CUP Archive* (1968).

[32]. Kármán, T. V. Über laminare und turbulente Reibung. *ZAMM - J. Appl. Math. Mech* **1,** 233–252 (1921).

[33]. Choi, S. U., & Eastman, J. A.. Enhancing thermal conductivity of fluids with nanoparticles (No. ANL/MSD/CP-84938; CONF-951135-29) (1995). *Argonne National Lab., IL (United States).*

[34]. Turkyilmazoglu, M. & Senel, P. Heat and mass transfer of the flow due to a rotating rough and porous disk. *Int. J. Therm. Sci*. **63**, 146–158 (2013).

[35]. Turkyilmazoglu, M. Nanofluid flow and heat transfer due to a rotating disk. *Comput. Fluids* **94**, 139–146 (2014).

[36]. Sheikholeslami, M. & Ganji, D. D. Three dimensional heat and mass transfer in a rotating system using nanofluid. *Powder Technol*. **253**, 789–796 (2014).

[37]. Sheikholeslami, M., Hatami, M. & Ganji, D. D. Nanofluid flow and heat transfer in a rotating system in the presence of a magnetic field. *J. Mol. Liq*. **190**, 112–120 (2014).

[38]. Hayat, T., Haider, F., Muhammad, T. & Alsaedi, A. Three-dimensional rotating flow of carbon nanotubes with Darcy-Forchheimer porous medium. *PlosONE* (2017) doi:10.1371/journal.pone.0179576.

[39]. Vajravelu, K. & Roper, T. Flow and heat transfer in a second grade fluid over a stretching sheet. *Int. J. Non. Linear. Mech.* **34**, 1031–1036 (1999).

[40]. Roşca, N. C. & Pop, I. Unsteady boundary layer flow over a permeable curved stretching/shrinking surface. *Eur. J. Mech. B/Fluids* **51**, 61–67 (2015).

[41]. Sajid, M., Ali, N., Javed, T., & Abbas, Z. Stretching a Curved

Surface in a Viscous Fluid. *Chinese Phys. Lett*. **27,** 24703–024703 (2010).

[42]. Wang, C. Y. Stretching a surface in a rotating fluid. *ZAMP Zeitschrift für Angew. Math. und Phys.* **39**, 177–185 (1988).

[43]. Hayat, T. & Hutter, K. Rotating flow of a second-order fluid on a porous plate. *Int. J. Non. Linear. Mech*. **39**, 767–777 (2004).

[44]. Hayat, T., Javed, T. & Sajid, M. Analytic solution for MHD rotating flow of a second grade fluid over a shrinking surface. *Phys. Lett. Sect. A Gen. At. Solid State Phys*. **372**, 3264–3273 (2008).

[45]. Rees, D. A. S. & Bassom, A. P. The Blasius boundary layer flow of a micropolar fluid. *Int. J. Eng. Sci*. **34**, 113–124 (1996).

[46]. Soundalgekar, V. M. & Takhar, H. S. Flow of micropolar fluid past a continuously moving plate. *Int. J. Eng. Sci*. **21**, 961–965 (1983).

[47]. Turkyilmazoglu, M. Nanofluid flow and heat transfer due to a rotating disk. *Comput. Fluids* **94**, 139–146 (2014).

[48]. Sugunamma, V., Reddy, J. V. R., Raju, C. S. K., Jayachandra Babu, M. & Sandeep, N. Effects of Radiation and Magnetic field on the flow and heat transfer of a nanofluid in a rotating frame. *Ind. Eng. Lett*. **4**, 8–14 (2014).

[49]. Pramanik, S. Casson fluid flow and heat transfer past an exponentially porous stretching surface in presence of thermal radiation. *Ain Shams Eng. J.* **5**, 205–212 (2014).

[50]. Cross, M. M. Rheology of non-Newtonian fluids: A new flow equation for pseudoplastic systems. *J. Colloid Sci*. **20,** 417–437 (1965).

[51]. Khan, M., Manzur, M. & Rahman, M. Boundary-layer flow and heat transfer of cross fluid over a stretching sheet. *Therm. Sci***. 23**, 307–318 (2019).

[52]. Hayat, T., Khan, M. I., Tamoor, M., Waqas, M. & Alsaedi, A. Numerical simulation of heat transfer in MHD stagnation point flow of Cross fluid model towards a stretched surface. *Results Phys*. **7**, 1824–1827 (2017).

[53]. Khan, M., Manzur, M. & ur Rahman, M. On axisymmetric flow and heat transfer of Cross fluid over a radially stretching sheet. *Results Phys.* **7**, 3767–3772 (2017).

[54]. Sultan, F., Khan, W. A., Ali, M., Shahzad, M., Irfan, M., & Khan, M. Theoretical aspects of thermophoresis and Brownian motion for three-dimensional flow of the cross fluid with activation energy. *Pramana - J. Phys*. **92**, 1–10 (2019).

[55]. M. Kumari and G. Nath, Bangalore, India MHD boundary-layer flow of a non-Newtonian fluid over a continuously moving surface with a parallel free stream. Acta Mechanica 146, 139 150 (2001)